HOKKAIDO UNIVERSITY

| | |
|---|---|
| Title | Characteristics of aerosol number concentrations over the ice-covered Okhotsk Sea |
| Author(s) | Inoue, Jun; Toyota, Takenobu |
| Citation | Journal of The Meteorological Society of Japan, 83(4), 633-640 |
| Issue Date | 2005-08 |
| Doc URL | http://hdl.handle.net/2115/5593 |
| Type | article (author version) |
| File Information | JMSJ83-4.pdf |

Instructions for use

Hokkaido University Collection of Scholarly and Academic Papers : HUSCAP

# Characteristics of aerosol number concentrations over the ice-covered Okhotsk Sea

**Jun Inoue**,
Institute of Observational Research for Global Change,
Japan Agency for Marine-Earth Science and Technology,
Yokosuka, Japan

**and**

**Takenobu Toyota**
Institute of Low Temperature Science,
Hokkaido University,
Sapporo, Japan

Corresponding author: Jun Inoue
Institute of Observational Research for Global Change
Japna Agency for Marine-Earth Science and Technology
2-15 Natsushima-cho
Yokosuka 237-0061, Japan
Phone: 046-867-9483; FAX: 046-867-9455
e-mail: jun.inoue@jamstec.go.jp

Submitted to *J. Meteor. Soc. Japan* on 12 October 2004
Accepted on 9 May 2005

# Abstract

Aerosol number concentrations were observed in conjunction with in-situ meteorological parameters aboard the patrol vessel SOYA in February 2003 over the ice-covered Okhotsk Sea. The concentrations of particles with radii larger than 0.35 $\mu$m were close to the background level, while concentrations of particles less than 0.35 $\mu$m were close to the remote continental level. During the observation period, relatively higher and lower aerosol number concentrations (HA and LA) were observed, depending on synoptic weather conditions. Backward trajectory analyses revealed that for the HA period, the air mass in the study region traced back to the Sea of Japan; for the LA period, the air mass originated from the northern ice-covered area. This suggests that sea ice influences the aerosol number concentration by suppressing the amount of oceanic sea salt supplied to air masses. Using the observational data and an empirical formula, differences in surface solar radiation between the HA and LA periods were also examined.

# 1 Introduction

As sea ice in the southern Sea of Okhotsk is situated at a relatively low latitude, solar radiation plays a significant role in the surface heat budget, even in mid-winter (Toyota and Wakatsuchi 2001). Therefore, it is important to estimate solar radiation in this region accurately to determine ice growth conditions. Aerosol has a considerable influence on irradiance in general, and may be one factor modifying solar radiation in this region. From surface meteorological data collected during winter 2001, Toyota et al. (2002) estimated a 0.02 atmospheric turbidity coefficient ($\beta$) in this region, and concluded that the atmosphere over the ice-covered area was significantly clean. As $\beta$ represents the attenuation of solar radiation owing to atmospheric aerosols, such a clean environment may relate to the presence of ice cover in the Sea of Okhotsk. Therefore, it is important to determine whether this result reflects a mere temporal event or a broader climatologic feature.

To grasp the variability of aerosol number concentrations under ice-covered situations, we monitored aerosols using an optical particle counter on board the patrol vessel (hereafter P/V) SOYA. The study region covered the southern Sea of Okhotsk, and observations took place over a 1-week period in the winter of 2003. Measured aerosols exceeded 0.15 $\mu$m in radius, a size range that can significantly affect irradiance. Concurrently, we monitored solar radiation with a pyranometer and sky conditions with forward- and upward-looking video cameras. We selected video images of clear skies and then examined the radiative effect of aerosols for each case.

# 2 Observation

Observations were conducted from 6−13 February 2003 in the southern Sea of Okhotsk. Fig-

ure 1 shows the cruise track. During the cruise, the aerosol number concentration and shortwave radiation were monitored in conjunction with meteorological observations. The number concentrations of aerosol particles (AP) were measured using an optical particle counter (RION Co., Ltd.; hereafter OPC), which automatically determines the size spectra of AP. The AP radii were divided into six size ranges: 0.15−0.25, 0.25−0.35, 0.35−0.5, 0.5−1, 1−2.5, and 2.5< r (r: radius in $\mu$m). The sampling time was from 0630 to 1630 local standard time (LST) at 5-minute intervals. The OPC was installed on the right side of the upper deck at a height 14.0 m above sea level to avoid contamination from the ship. Pyranometers (MR-40 type designed by EKO Instruments Co., Ltd.) were used to measure shortwave radiation. The pyranometers measure upward and downward shortwave radiation in the 305- to 2800-nm wavelength range with an accuracy of ±2%. Sources of the measurement error on the ship has been examined by Toyota et al. (1999).

Supplementary data included sky-monitoring images recorded at 1-minute intervals by three video cameras installed on the ship's upper deck. Two video cameras monitored adjacent front views of the sky; each camera had a 30 ° field of view. The third camera observed the zenith view of the sky. Although the monitoring width was limited, these views represent sky conditions to an extent, since the two front images viewed the sky that would be overhead a few minutes after the ship moved on. Furthermore, rearward cloud conditions were also checked with hourly visual observations. The video images were used to select cloud-free conditions for analyzing aerosol and radiation data.

During the observation period, the southern Sea of Okhotsk was mostly covered with sea ice (Fig. 1). The air temperature increased gradually during the first half of the observation period, in association with a cyclone approaching northern Japan on 9−10 February (Fig. 2a). Synoptic

variability was better characterized by the water vapor mixing ratio than by air temperature, because of the small diurnal variation of water vapor (Fig. 2d); the lower mixing ratio at the beginning and end of the observation period (6 and 12−13 February) reflects the cold, dry situation created by the winter monsoon, whereas the higher mixing ratio in the middle of the observation period (9−10 February) reflects the warm, wet air mass associated with the approach and passage of a cyclone. Solar radiation (Fig. 2f) and cloud monitoring observations showed frequent fair-sky conditions during the cruise, except on 9−10 February.

# 3 Results

The number concentrations of AP for six specified size ranges (r = 0.15−0.25, 0.25−0.35, 0.35−0.5, 0.5−1, 1−2.5, and 2.5 < r) are shown in Fig. 3. The maximum AP concentration was observed on 10 February, reflecting an increase of approximately one order of magnitude compared with the concentration measured on 6 February. In the latter half of the observation period (10−13 February), the AP number concentration decreased. This trend in the AP number concentration seems to correspond to changes in the air temperature and vapor mixing ratio (Figs. 2a, d). The relationship between the water vapor mixing ratio and AP number concentration for the 0.25−0.35 $\mu$m particles is plotted in Fig. 4. Obviously, the AP number concentration correlates with the water vapor mixing ratio well. In addition to this, the two groups can be clearly distinguished; open circles show period I (6−9 February), and closed circles represent period II (10−13 February). This feature was more significant on 13 February especially in relatively large particle size ranges (Fig. 3) although the meteorological conditions (i.e., air temperature and humidity) were nearly restored to earlier conditions observed on 6 February (Fig. 2).

To examine differences in the size distributions between periods I and II, the size distribution dN/d(log r) averaged for each period is depicted as a function of particle radius r in Fig. 5a. The size distributions for both periods are similar to Junge's (1952) distribution. Figure 5a also depicts the distribution of the AP number concentrations, which were calculated using the empirical formula from Jaenicke (1993). The observed AP size distributions are close to the background level (i.e., tropospheric aerosols in the free atmosphere), particularly for the relatively large particle size ($\geq$0.35$\mu$m). The AP number concentration in period II is also significantly higher than that in the period I; in addition, the difference in the AP size distribution increases with particle size. AP smaller than 0.35$\mu$m are likely affected by continental aerosols due to their long-range transport.

To examine the cause of differences in the AP size distribution between periods I and II, the correlation coefficient between the AP number concentration and the water vapor mixing ratio was calculated for each size range (Fig. 5b). In each period, the correlation coefficient is significant for each AP size range at more than 99 %. In period I, the correlation coefficients were as high as 0.8 for all size ranges, suggesting that the AP number concentration is closely related to synoptic weather conditions. In period II, however, the values decreased with increasing particle size. This suggests that other sources/sinks changed the AP number concentration.

# 4 Trajectory analysis

To understand the cause of differences in the AP size distribution between periods I and II, the air-mass transport process was examined using backward trajectory analysis. The analysis is based on the Hybrid Single-Particle Lagrangian Integrated Trajectory (HYSPLIT) model developed by

NOAA (Draxier and Rolph 2003; Rolph 2003). This model includes the vertical motion mode with meteorological data from the National Centers for Environmental Prediction Final Analyses (NCEP FNL). Daily, each trajectory was traced backward for three days using the position of the SOYA at 0000 and 1200 UTC. The initial heights were set to 10 and 500 m to approximate the surface (i.e., the height of the OPC installed on the SOYA) and upper boundary layers, respectively.

Figure 6 depicts the trajectories calculated at the two levels. Note that at both levels, most of the period II air masses had passed over the Sea of Japan within one day before reaching SOYA, and air flow was almost barotropic between the two levels (closed circles in Figs. 6a, b). By contrast, for period I, half of the air masses at the lower level came from Sakhalin Island or areas of northern ice cover (open circles in Fig. 6a). A few air masses crossed the Sea of Japan. However, these air masses spent more than one day over the Sea of Japan before arriving at the study area (open circles in Fig. 6a). The two levels show significantly different trajectories. These results suggest that in period II the boundary layer was well mixed and the surface air was carried upward in the atmosphere; in period I, the surface air was limited to the lower level.

Generally, the Sea of Japan has very strong whitecaps associated with breaking waves during cold-air outbreaks (e.g., Ebuchi 1999). Under such conditions, sea-salt particles are formed by bursting air bubbles at the sea surface. These particles formed over a wide area and are carried into the lower boundary layer (e.g., Kikuchi et al. 2003). By contrast, during period I, the supply of sea-salt particles to the air mass was likely suppressed by ice cover or a relatively weak monsoon. In such a situation, relatively large AP would decrease by falling from the air mass, even if supplied with large AP from seawater. This suggests that air passing over the ice-covered

Okhotsk Sea during period I contained a smaller amount of sea-salt particles than that passing over in period II. These speculations are supported by the fact that the difference in AP size distribution increases with particle size (Fig. 5a).

The effect of synoptic weather conditions on the AP number concentration has been noted in other marginal ice zones. During the East Greenland Sea Marginal Ice Zone Experiment of 1983, Borrmann et al. (1987) compared the AP number concentration in the marginal ice zone before and after passage of a cold front. They found a significant decrease in AP with radii larger than 0.9 $\mu$m when the wind direction changed from air flow from open sea to air flow from ice cover. This finding suggests that the open ocean supplies a greater amount of sea-spray AP, while a smaller concentration of AP results from air over the ice cover.

The clean air observed over the ice cover on 20 February 2001 described in Toyota et al. (2002) could presumably be categorized with the clean air observed in period I of our study. The backward trajectory for 2001 (triangles in Fig. 6) resembles that in period I. The transport speed was relatively slow over the ice cover and the paths are quite different at the two levels, suggesting the existence of a shallow cold air mass over ice cover. When a cold air mass dominates over ice cover, which induces the northeasterly wind formed by the pressure gradient between the relatively warm Sea of Japan and cold Okhotsk Sea (e.g., Fujiyoshi et al. 1996), convergence cloud bands often appear off the west coast of Hokkaido. This may be a good optical indicator for distinguishing air mass properties. Therefore, the AP size distribution in the southern Sea of Okhotsk is differently modified according to two types of air-mass trajectories. One trajectory takes air masses over the Sea of Japan and is associated with a strong monsoon; the other moves over ice cover in the Sea of Okhotsk.

# 5 Discussion

Several studies have reported observations of aerosols in the polar regions (e.g., Shaw 1982; Ito 1982; Ito et al. 1986). For example, by monitoring aerosols at Syowa Station, Antarctica, Ito (1982) showed that the variability in aerosol amounts greater than 0.1 $\mu$m might have originated from ocean and was largely controlled by cyclonic activity. As Shine (1984) pointed out, high albedo areas have multiple reflections, which create a different radiative flux than in low albedo areas; consequently, the presence of aerosols can influence solar radiation. Although many researchers have examined surface shortwave forcing by aerosols (e.g., Nakajima et al. 1996; Takayabu et al. 1999), many studies focused on snow-free areas. As described by the Intergovernmental Panel on Climate Change (IPCC 2001), the aerosols and sea-ice cover are important factors in global climate change. Therefore, our study might contribute basic data on the climate system in polar/sub-polar regions.

To examine the effect of aerosols on solar radiation, we discuss how the difference in AP between periods I and II affects surface solar radiation. Figure 7 shows the observed global solar radiation (closed circles) as a function of the optical path length of an air mass as $M = (p/1013.2)\sec\theta$, where $p$ is the surface pressure in hPa, and $\theta$ is the solar zenith angle. To exclude cloud effects, we extracted cloud-free images from the forward- and upward-looking cameras. Reference global solar radiation estimated using an empirical formula (Kondo and Miura 1983) with different turbidity coefficients ($\beta = 0.00$, 0.01, 0.04) is superimposed on this figure. For this calculation, the observed albedo (10-minute averaged values, corresponding to a few kilometers) and solar zenith angle were used. Further, the precipitable water ($w^*$ in kg m$^{-2}$) was estimated by regression ($w^* = 1.396e_a - 0.356$: RMS = 0.645 kg m$^{-2}$) with observed surface vapor pressure ($e_a$ in hPa)

(Toyota et al. 2002). This regression was derived from sonde observations conducted in the study area during the same seasons for 1998−2000 (e.g., Inoue et al. 2003). For the case of 1.5 g kg$^{-1}$ of water vapor mixing ratio at $M = 2.5$ (Figs. 7a, b), the amount of observed surface solar radiation was close to the estimated value at $\beta = 0.01$ and 0.04 in periods I and II, respectively. The plotted data are mostly on the same $\beta$ line for each case, suggesting that the difference in solar radiation between periods I and II (approximately 20 W m$^{-2}$) was caused by differences in the aerosol number concentration. Such an effect becomes small under relatively moist conditions (approximately 10 W m$^{-2}$ at $M = 3.1$: Figs. 7c, d). The amount of the aerosol radiative effect ($F = 10-20$ W m$^{-2}$) corresponds to the ice growth rate of 0.3−0.6 cm day$^{-1}$ ($= F/(\rho_i L_f)$, where $\rho_i$ is the ice density, and $L_f$ is the latent heat of fusion), and is almost comparable with the daily mean sea-ice growth rate in the southern Sea of Okhotsk (Toyota et al. 2000; Inoue et al. 2001).

However, errors in the empirical formula and observed global solar radiation cause some uncertainty in the derived AP radiative effect. For example, observed global solar radiation with 300−400 W m$^{-2}$ has an uncertainty of 6−8 W m$^{-2}$ arising from pyranometer accuracy (±2%). Both the 10-minute averaged albedo (RMS = 0.11) and precipitable water (RMS = 0.645 kg m$^{-2}$) used in the empirical formula cause a ±1% uncertainty in the radiation value. Although the sum of these errors is nearly comparable with the radiative effect of AP as estimated above, the intercomparison between the two periods seems valid because their solar altitudes are almost the same and the error caused by the accuracy of the instrument can be canceled.

# 6 Summary

In early February 2003 over the ice-covered Okhotsk Sea, number concentrations of aerosol

particles were observed in conjunction with in-situ meteorological observations aboard the P/V SOYA. During the observation period, two major winter monsoon events occurred. The results showed that size distributions larger than 0.35 $\mu$m were close to the background level, suggesting that the atmosphere is basically clean in this region. The AP number concentrations correlated with synoptic-scale variability; this relationship was divided into two categories: period I with lower aerosol concentrations (6−9 February) and period II with higher aerosol concentrations (10−13 February). Backward trajectory analysis revealed that period II was characterized by an air mass advected over the Sea of Japan, suggesting that sea salt originating from wind-formed waves was transported to the shallow atmospheric boundary layer during air mass modification. Period I was characterized by air masses originating over northern ice cover or transported slowly from the Sea of Japan. Based on the observational data and an empirical formula, differences in surface solar radiation between the periods I and II were also discussed. Further observations using a sky radiometer or sunphotometer will be necessary for better estimating the radiative effect of AP over ice-covered regions. Moreover, future investigations will be desired to identify the chemical composition of individual aerosol particles.

# Acknowledgments

We are sincerely grateful to the crew of P/V SOYA of the Japan Coast Guard and our colleagues at ILTS for their kind cooperation throughout the cruise. Thanks are also extended to all the scientists who conducted ice observations on board the SOYA. The OPC instrument for observing the aerosol number concentration was provided by Y. Fujiyoshi. MODIS satellite imagery was obtained from JAXA/Tokai University. The authors gratefully acknowledge the NOAA Air

Resources Laboratory (ARL) for providing the HYSPLIT transport and dispersion model and the READY web site (http://www/arl.noaa.gov/ready.html) used in this publication. The beneficial comments by J. A. Curry and two anonymous reviewers are also acknowledged.

# References


Borrmann, S. H., K. L. Davidson and M. E. Miller, 1987: Aerosol size distributions in the marginal ice zone during the 1983 Marginal Ice Zone Experiment. *J. Geophys. Res*, **92**, 6971–6976.

Draxler, R R. and G. D. Rolph, 2003: HYSPLIT (HYbrid Single-Particle Lagrangian Integrated Trajectory) Model access via NOAA ARL READY Website

(http://www.arl.noaa.gov/ready/hyspit4.html). NOAA Air Resource Laboratory, Silver Spring, MD.

Ebuchi, N., 1999: Growth of wind waves with fetch in the Sea of Japan under winter monsoon investigated using data from satellite altimeters and scatterometer. *J. Oceanogr.*, **55**, 575–584.

Fujiyoshi, Y., Y. Kodama, K. Tsuboki, K. Nishimura and N. Ono, 1996: Structures of cold air during the development of a broad band cloud and a meso-$\beta$-scale vortex: Simultaneous two-point radiosonde observations. *J. Meteor. Soc. Japan*, **74**, 281–297.

Inoue, J., M. Honda and M. Kawashima, 2001: Air mass transformation processes over the southwestern region of the ice-covered Sea of Okhotsk during cold air outbreaks. *J. Meteor. Soc. Japan*, **79**, 657-670.

—, J. Ono, Y. Tachibana, M. Honda, K. Iwamoto, Y. Fujiyoshi and K. Takeuchi, 2003: Characteristics of heat transfer over the ice-covered Sea of Okhotsk during cold air outbreaks. *J. Meteor. Soc. Japan*, **81**, 1057-1067.

IPCC, 2001: *Climate Change 2001, The Scientific Basis*, Cambridge University Press, Cambridge, 896pp.

Ito, T., 1982: On the size distribution of submicron aerosols in the Antarctic atmosphere. *Antarctic Record*, **76**, 1–19 (in Japanese with English summary).

—, Y. Morita and Y. Iwasaka, 1986: Balloon observation of aerosols in the Antarctic troposphere and stratosphere. *Tellus*, **38B**, 214–222.

Jaenicke, R., 1993: Tropospheric aerosols, *Aerosol-cloud-climate interactions*, edited by P. V. Hobbs, Academic Press, 1-27.

Junge, C. E., 1952: Die Konstitution des atmospharischen Aerosols. *Ann. Meteorologie Beiheft*, **5**, 1-55.

Kikuchi, K., S. Matsumoto, H. Uyeda, O. Kikuchi and D. I. Lee, 2003: Relationship between aerosol number concentrations and convergence fields in winter monsoon seasons. *J. Geophys. Res.*, **108**, 4115, doi:1029/2001JD001271.

Kondo, J. and A. Miura, 1983: Empirical formula of the solar radiation at the ground level and a simple method to examine an inaccurate pyranometer. *Tenki*, **30**, 469-475 (in Japanese).

Nakajima, T., T. Hayasaka, A. Higurashi, G. Hashida, N. Moharram-Nejad, Y. Najafi and H. Valavi, 1996: Aerosol optical properties in the Iranian Region obtained by ground-based solar radiation measurements in the summer of 1991. *J. Appl. Meteor.*, **35**, 1265–1278.

Rolph, G. D., 2003: Real-time Environmental Applications and Display sYstem (READY) Website (http://www.arl.noaa.gov/ready/hyspit4.html). NOAA Air Resource Laboratory, Silver Spring, MD.

Shaw, G. E., 1982: Atmospheric turbidity in the polar regions. *J. Appl. Meteor.*, **21**, 1080–1088.

Shine, K. P., 1984: Parameterization of the shortwave flux over high albedo surfaces as a function of cloud thickness and surface albedo. *Quart. J. Roy. Meteor. Soc.*, **110**, 747–764.

Takayabu, Y. N., T. Ueno, T. Nakajima, I. Matsui, Y. Tsushima, K. Aoki, N. Sugimoto and I. Uno, 1999: Estimate of the cloud and aerosol effects on the surface radiative flux based on the measurements and the transfer model calculations, Part I: Shortwave forcing at Tateno, Japan. *J. Meteor. Soc. Japan*, **77**, 1007–1021.

Toyota, T., J. Ukita, K. I. Ohshima, M. Wakatsuchi and K. Muramoto, 1999: A measurement of sea ice albedo over the southwestern Okhotsk Sea. *J. Meteor. Soc. Japan*, **77**, 117–133.

—, T. Kawamura and M. Wakatsuchi, 2000: Heat budget in the ice cover of the Southern Okhotsk Sea derived from in-situ observations. *J. Meteor. Soc. Japan*, **78**, 585–596.

— and M. Wakatsuchi, 2001: Characteristics of the surface heat budget during the ice-growth season in the southern Sea of Okhotsk. *Ann. Glaciol.*, **33**, 230–236.

—, K. Baba, E. Hashiya and K. I. Ohshima, 2002: In-situ ice and meteorological observations in the southern Sea of Okhotsk in 2001 winter: ice structure, snow on ice, surface temperature, and optical environments. *Polar Meteor. Glaciology*, **16**, 116–132.

# Figure Captions

Figure 1: Cruise track (white line) and MODIS satellite imagery on 7 February 2003.

Figure 2: Time series of (a) air temperature, (b) surface brightness temperature, (c) relative humidity, (d) water vapor mixing ratio, (e) real wind speed, and (f) solar radiation.

Figure 3: Time series of the aerosol number concentration at each particle size range (0.15−0.25, 0.25−0.35, 0.35−0.5, 0.5−1, 1−2.5, 2.5 < r: $\mu$m).

Figure 4: Scatter plots of the water vapor mixing ratio and aerosol number concentration (0.25−0.35). Open circles for 6−9 Feb. (period I) and closed circles for 10−13 Feb. (period II).

Figure 5: (a) Size distributions of aerosol particles, and (b) correlation coefficients between the aerosol number concentration and the water vapor mixing ratio in period I (open) and II (closed). Four curves from Jaenicke (1993) indicate the modeled number size distributions for polar, background, maritime, and remote continental aerosols.

Figure 6: Results of the backward trajectory analysis at initial heights of (a) 10 and (b) 500 m. There is a 12-hour time resolution between successive marks.

Figure 7: Observed (dots) and estimated (solid lines) surface solar radiation under clear-sky conditions as a function of the optical path length of air mass for water vapor mixing ratios of (a, b) 1.5 g $kg^{-1}$ and (c, d) 2.4 g $kg^{-1}$.

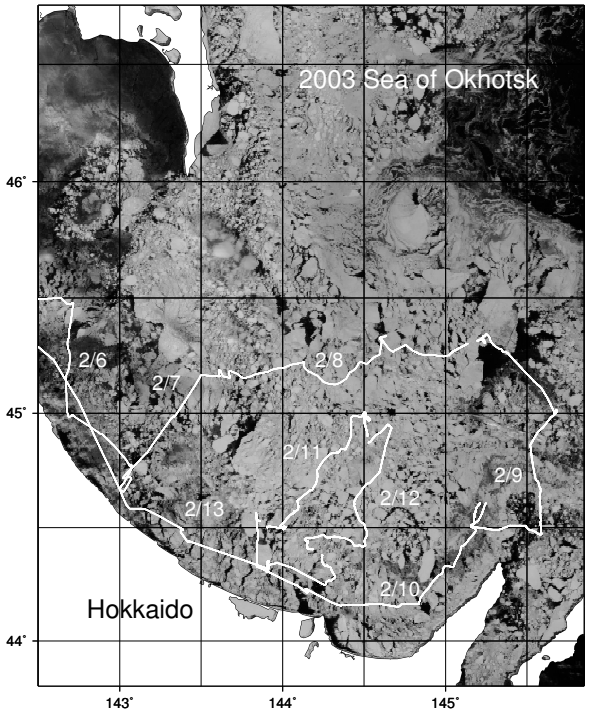


Figure 1: Cruise track (white line) and MODIS satellite imagery on 7 February 2003.

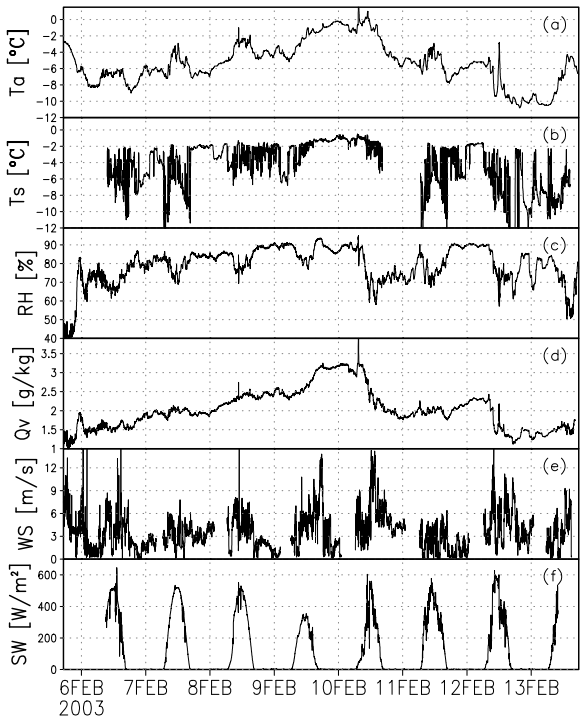


Figure 2: Time series of (a) air temperature, (b) surface brightness temperature, (c) relative humidity, (d) water vapor mixing ratio, (e) real wind speed, and (f) solar radiation.

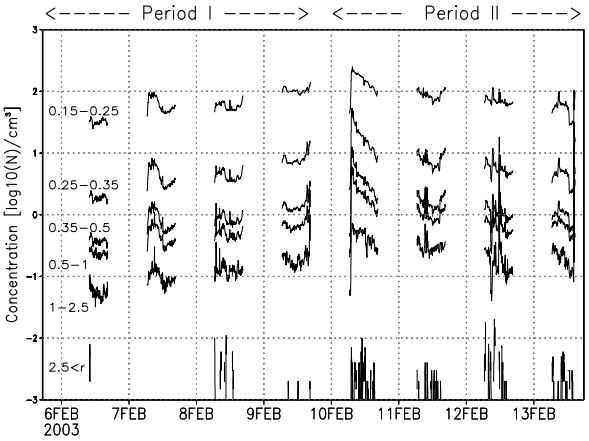


Figure 3: Time series of the aerosol number concentration at each particle size range (0.15−0.25, 0.25−0.35, 0.35−0.5, 0.5−1, 1−2.5, 2.5 < r: $\mu$m).

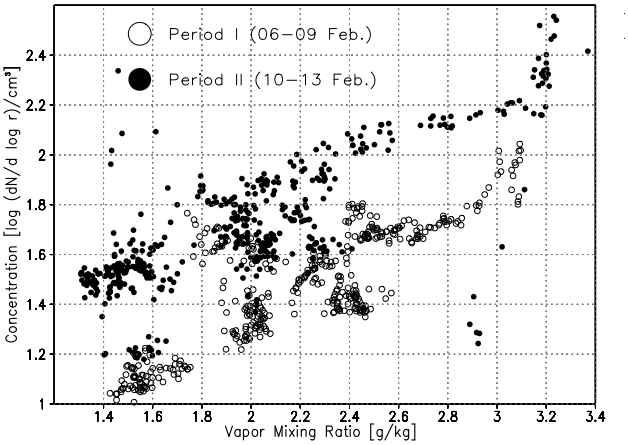


Figure 4: Scatter plots of the water vapor mixing ratio and aerosol number concentration (0.25−0.35). Open circles for 6−9 Feb. (period I) and closed circles for 10−13 Feb. (period II).

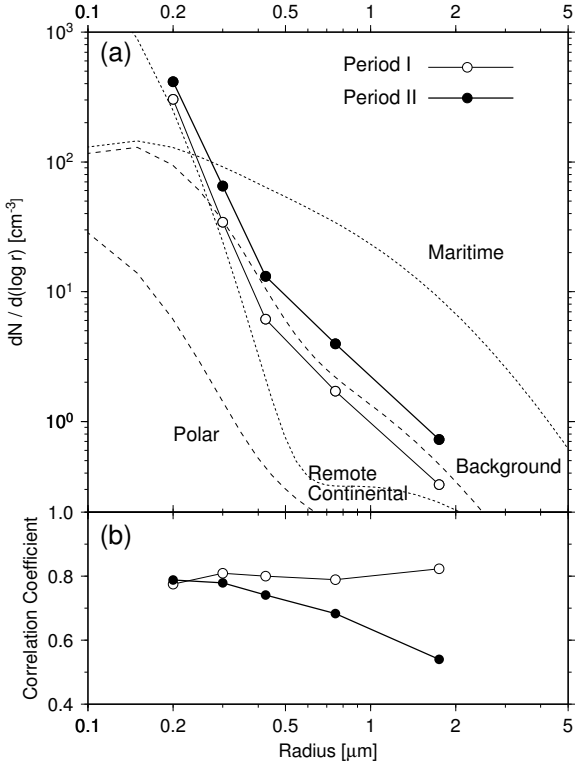


Figure 5: (a) Size distributions of aerosol particles, and (b) correlation coefficients between the aerosol number concentration and the water vapor mixing ratio in period I (open) and II (closed). Four curves from Jaenicke (1993) indicate the modeled number size distributions for polar, background, maritime, and remote continental aerosols.

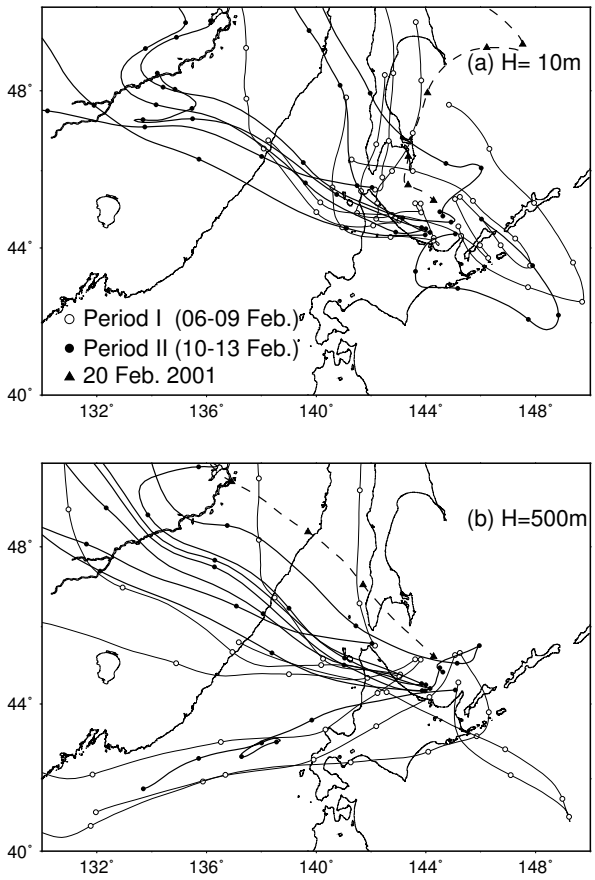


Figure 6: Results of the backward trajectory analysis at initial heights of (a) 10 and (b) 500 m. There is a 12-hour time resolution between successive marks.

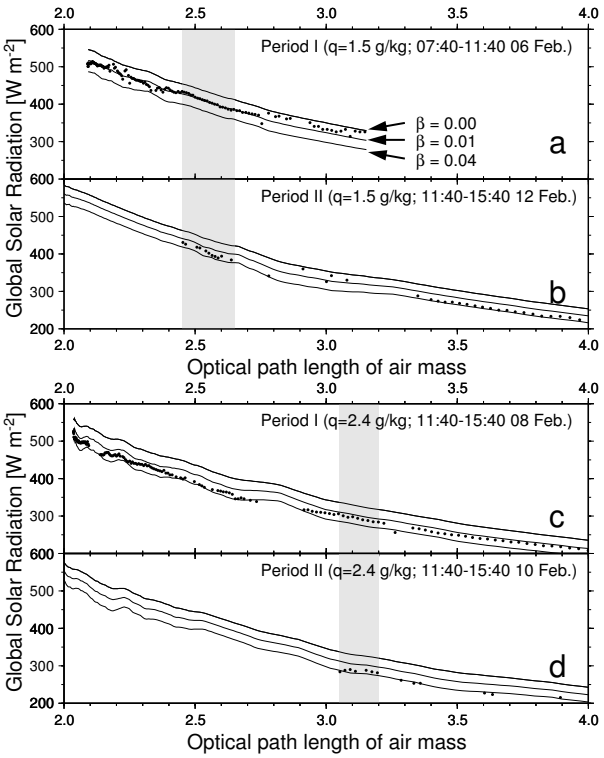


Figure 7: Observed (dots) and estimated (solid lines) surface solar radiation under clear-sky conditions as a function of the optical path length of air mass for water vapor mixing ratios of (a, b) 1.5 g $kg^{-1}$ and (c, d) 2.4 g $kg^{-1}$.